ARTICLE

Early postmortem brain MRI findings in COVID-19 non-survivors

Tim Coolen, MD,* Valentina Lolli, MD,* Niloufar Sadeghi, MD, PhD, Antonin Rovai, PhD, Nicola Trotta, PhD, Fabio Silvio Taccone, MD, PhD, Jacques Creteur, MD, PhD, Sophie Henrard, MD, Jean-Christophe Goffard, MD, PhD, Olivier Dewitte, MD, PhD, Gilles Naeije, MD, PhD, Serge Goldman, MD, PhD, and Xavier De Tiège, MD, PhD

Correspondence
Dr. De Tiège
xdetiege@ulb.ac.be

Neurology® 2020;95:e2016-e2027. doi:10.1212/WNL.0000000000010116

Abstract

Objectives

The severe acute respiratory syndrome coronavirus 2 (SARS-CoV-2) is considered to have potential neuroinvasiveness that might lead to acute brain disorders or contribute to respiratory distress in patients with coronavirus disease 2019 (COVID-19). This study investigates the occurrence of structural brain abnormalities in non-survivors of COVID-19 in a virtopsy framework.

Methods

In this prospective, monocentric, case series study, consecutive patients who fulfilled the following inclusion criteria benefited from an early postmortem structural brain MRI: death <24 hours, SARS-CoV-2 detection on nasopharyngeal swab specimen, chest CT scan suggestive of COVID-19, absence of known focal brain lesion, and MRI compatibility.

Results

Among the 62 patients who died of COVID-19 from March 31, 2020, to April 24, 2020, at our institution, 19 decedents fulfilled the inclusion criteria. Parenchymal brain abnormalities were observed in 4 decedents: subcortical microbleeds and macrobleeds (2 decedents), cortico-subcortical edematous changes evocative of posterior reversible encephalopathy syndrome (PRES; 1 decedent), and nonspecific deep white matter changes (1 decedent). Asymmetric olfactory bulbs were found in 4 other decedents without downstream olfactory tract abnormalities. No brainstem MRI signal abnormality was observed.

Conclusions

Postmortem brain MRI demonstrates hemorrhagic and PRES-related brain lesions in non-survivors of COVID-19. SARS-CoV-2–related olfactory impairment seems to be limited to olfactory bulbs. Brainstem MRI findings do not support a brain-related contribution to respiratory distress in COVID-19.

MORE ONLINE

COVID-19 Resources
For the latest articles, invited commentaries, and blogs from physicians around the world
NPub.org/COVID19

*These authors contributed equally to this work.

From the Department of Radiology (T.C., V.L., N.S.), Department of Nuclear Medicine (A.R., N.T., S.G., X.D.T.), Intensive Care Unit (F.S.T., J.C.), Department of Internal Medicine (S.H., J.-C.G.), Department of Neurosurgery (O.D.W.), and Department of Neurology (G.N.), CUB Hôpital Erasme, and Laboratoire de Cartographie fonctionnelle du Cerveau (T.C., V.L., A.R., N.T., S.G., X.D.T.), UNI–ULB Neuroscience Institute, Université libre de Bruxelles, Brussels, Belgium.

Go to Neurology.org/N for full disclosures. Funding information and disclosures deemed relevant by the authors, if any, are provided at the end of the article.

Glossary

ACD = apparent diffusion coefficient; **ACE2** = angiotensin-converting enzyme 2; **CAA** = cerebral amyloid angiopathy; **COVID-19** = coronavirus disease 2019; **DIC** = disseminated intravascular coagulation; **DWI** = diffusion-weighted imaging; **FA** = flip angle; **FLAIR** = fluid-attenuated inversion recovery; **FOV** = field of view; **ICU** = intensive care unit; **MR** = magnetic resonance; **PRES** = posterior reversible encephalopathy syndrome; **SARS-CoV-2** = severe acute respiratory syndrome coronavirus 2; **SVD** = small vessel disease; **SWI** = susceptibility-weighted imaging; **TE** = echo time; **TI** = inversion time; **T1WI** = T1-weighted imaging; **TR** = repetition time; **T2WI** = T2-weighted imaging.

Infection by the severe acute respiratory syndrome coronavirus 2 (SARS-CoV-2), called coronavirus disease 2019 (COVID-19) by the World Health Organization, is associated with an ongoing worldwide outbreak of atypical and severe pneumonia.[1,2]

SARS-CoV-2 uses human cell receptor angiotensin-converting enzyme 2 (ACE2) as cellular entry point.[3] ACE2 is expressed in airway epithelia, lung parenchyma, vascular endothelium, heart, kidneys, and small intestine,[4] which explains most of the COVID-19 symptoms. ACE2 is also present in glial cells and neurons of mammalian brain, especially in brainstem nuclei involved in cardiorespiratory function.[4] SARS-CoV-2 is therefore considered to have potential neuroinvasiveness that might lead to acute brain disorders or contribute to respiratory distress in patients with COVID-19.[5,6] SARS-CoV-2 might enter the CNS through hematogenous dissemination or neuronal retrograde route via, for example, olfactory bulbs or medullary neurons.[6] The anosmia frequently observed in SARS-CoV-2–infected patients[7,8] supports the neural retrograde hypothesis. The neuroinvasiveness of SARS-CoV-2 is also supported by case reports of meningoencephalitis,[9–11] intracerebral hemorrhage,[12] ischemic strokes,[13] and secondary acute necrotizing encephalopathy[14] associated with SARS-CoV-2 infection. Central neurologic symptoms (e.g., headache, stroke, impaired consciousness) are also observed in 25% of patients with COVID-19.[15] Still, brain MRI data are scarce in patients with COVID-19 due to difficulties in obtaining such an examination in infected unstable patients during the COVID-19 outbreak.[15]

This prospective, monocentric, postmortem brain MRI case series investigated the occurrence of structural brain abnormalities in non-survivors of COVID-19 in a brain virtopsy framework performed early (≤24 hours) after death. We specifically searched for signs of acute brain injury (e.g., stroke, encephalitis) and MRI signal abnormalities along the olfactory tract and brainstem.

Methods

Study design and participants

From March 31, 2020, to April 24, 2020, consecutive decedents who fulfilled the following inclusion criteria were included: death <24 hours, SARS-CoV-2 detection (direct antigen detection or reverse transcriptase PCR) on nasopharyngeal swab specimen, chest CT scan suggestive of COVID-19 without alternative diagnosis, absence of known focal brain lesion, and MRI compatibility. Clinical data were retrieved from decedents' medical records and reviewed by clinicians (F.S.T., S.H., J.C.G., G.N., O.D.).

After death, decedents were directly placed in an MRI-compatible mortuary bag, brought to the morgue, and placed in dedicated mortuary refrigerators (2°C–3°C).

Standard protocol approvals, registrations, and patient consents

This study was carried out at the CUB Hôpital Erasme (Brussels, Belgium) after approval by the institutional Ethics Committee (reference: P2020/204, SRB2020121), which did not request informed consent from legal representatives.

Clinical definitions

Bilateral chest infiltrates associated with a Pa_{O_2}/Fi_{O_2} < 300 in ambient oxygen conditions or oxygen saturation <90% during administration of at least 50% oxygen fraction (Fi_{O_2}) were identified as severe respiratory failure. Acute kidney injury was defined according to the Kidney Disease Improving Global Outcomes criteria.[16] Hypoxic hepatitis was defined as an increase in aspartate or alanine transaminases >20 times the upper normal range (≤50 IU/L), that is, >1,000 IU/L in the setting of acute cardiovascular failure and in the absence of another cause of cell necrosis.[17] Disseminated intravascular coagulation (DIC) was defined according to standard criteria.[18] Acute cardiac injury associated with COVID-19 was identified according to recently proposed definitions.[19]

MRI data acquisition

Postmortem structural brain MRIs were performed on a 3T hybrid PET–magnetic resonance (MR) scanner (SIGNA, GE Healthcare, Chicago, IL) in accordance with COVID-19 institutional hygienic and safety rules. During the COVID-19 outbreak, the PET-MR facility was isolated from the rest of the Nuclear Medicine Department and dedicated to research investigations on COVID-19. This avoided any interference with ongoing clinical activities of the department. Mortuary bags were not opened during the procedure.

MRI sequences consisted of whole-brain axial 3D T1-weighted imaging (T1WI; repetition time [TR]/echo time [TE]/flip angle [FA] 8 milliseconds/3 milliseconds/12°, inversion time [TI] 450 milliseconds, field of view [FOV] 24 × 24 cm, matrix 240 × 240, resolution 1 × 1 × 1 mm), axial T2-weighted imaging

(T2WI; TR/TE/FA 6,500 milliseconds/126 milliseconds/142°, FOV 24 × 24 cm, matrix 480 × 480, resolution 0.5 × 0.5 × 3 mm, slice spacing 0.3 mm), sagittal 3D T2WI fluid-attenuated inversion recovery (FLAIR; TR/TE/FA 7,200 milliseconds/120 milliseconds/90°, TI 1,333–2,041 milliseconds, FOV 25.6 × 25.6 cm, matrix 256 × 256, resolution 1 × 1 × 1.4 mm), axial 3D susceptibility-weighted imaging (SWI; TR/TE/FA 48 milliseconds/25 milliseconds/10°, FOV 24 × 24 cm, matrix 240 × 240, resolution 1 × 1 × 1.6 mm), and axial diffusion-weighted imaging (DWI; TR/TE/FA 6,500 milliseconds/80 milliseconds/90°, FOV 25.6 × 25.6 cm, matrix 128 × 128, resolution 2 × 2 × 4 mm, slice spacing 0.4 mm). The TI of the 3D T2WI FLAIR sequence was adapted for each patient because this parameter depends strongly on the decedent's body temperature,[19,20] which was dependent on the time spent by decedents in mortuary refrigerators. In our case, TI was adapted in a trial-and-error fashion to minimize the CSF signal, except for D1. A coronal T2WI (TR/TE/FA 6,500 milliseconds/112 milliseconds/142°, FOV 15 × 15 cm, matrix 256 × 256, resolution 0.6 × 0.6 × 3 mm, slice spacing 0.2 mm) centered on olfactory bulbs completed the acquisition. Total acquisition time was ≈40 minutes.

MRI data analyses

MRI data were first independently reviewed by 3 neuroradiologists (V.L., T.C., N.S.) according to systematic and comprehensive visual assessment. Final reports were then discussed with 3 neurologists (S.G., X.D.T., G.N.) and with other clinicians (F.S.T., S.H., J.C.G., O.D.).

Brain MRI findings reflecting postmortem changes

MRI data were first screened for signal abnormalities that could be confidently attributed to early postmortem changes according to the existing literature.[21–24] Reported findings include increased T1WI signal of basal ganglia and thalami, suppression of fat signal intensity on T2WI, increased signal intensity of the cortical ribbon and the ventricular wall on DWI, and globally reduced apparent diffusion coefficient (ADC) values in the brain parenchyma. MRI data were also screened for potential additional postmortem changes, which, to the best of our knowledge, have not been reported. The increase in T1WI signal intensity was classified as absent (0), mild (1), or marked (2). The suppression of fat on T2WI was categorized as incomplete (1) or complete (2). The cortical and periventricular rim-like increased signal intensity on DWI was also classified as incomplete (1) or complete (2). ADC values were measured by using 3 ellipsoid regions of interest in the left centrum semiovale, left thalamus/lenticular/caudate nuclei, and left cerebellum.

Assuming that most postmortem MRI signal changes were related to changes in body temperature and therefore changes in T1 and T2 relaxation times of tissues, we postulated that signal abnormalities might increase with the delay between death and MRI data acquisition. We therefore performed Spearman rank correlation between scan delay and adjusted FLAIR TI needed for adequate water suppression (excluding D1), T1 increased signal intensity, T2WI fat suppression, and DWI increased signal intensity scores, as well as the sum of ADC values. Correlation results were considered significant for $p < 0.05$ corrected for multiple comparisons.

Brain MRI findings reflecting antemortem changes

MRI data were subsequently screened for signal abnormalities reflecting antemortem changes. These were divided into recent (i.e., potentially related to COVID-19) and long-standing (i.e., unlikely related to COVID-19) changes. Recent changes included hemorrhages, edema, and olfactory cleft and bulb abnormalities. Hemorrhages were considered recent if hyperintense on T1WI or in the absence of signal abnormality suggestive of cerebral amyloid angiopathy (CAA) or small vessel disease (SVD).[25] Long-standing signal abnormalities included white matter changes with an imaging pattern suggestive of microvascular ischemic chronic disease, enlargement of perivascular spaces, cerebral atrophy, and late-stage lacunar ischemic or hemorrhagic changes. The severity of T2/FLAIR white matter hyperintensities of presumed vascular origin was coded according to the Fazekas scale from 0 to 3 on T2WI and T2WI FLAIR sequences.[26] Basal ganglia and centrum semiovale enlargement of perivascular spaces was rated with a total score ranging from 0 to 8 on axial T2WI sequences.[27,28] Cerebral atrophy was assessed both by using the simplified global cortical atrophy score,[29] retaining the worst (highest) score across the brain, and by calculating the Evan index[30] on 3D T1WI sequences. Supratentorial and infratentorial cortical sequelae and deep lacunes, pontine microischemic leukoencephalopathy, and presumed old microhemorrhages or macrohemorrhages were also noted.

Data availability

Deidentified postmortem brain MRI data can be shared on reasonable request for scientific purpose and after approval of the CUB Hôpital Erasme Ethics Committee and authorities.

Results

Table 1 summarizes included decedents' characteristics. Clinical and biological data of included decedents are detailed in table e-1 available from Dryad, doi.org/10.5061/dryad.4qrfj6q7p.

Among the 62 patients who died of COVID-19 infection during the inclusion period, 19 decedents fulfilled the inclusion criteria. The time interval between death and MRI acquisition varied between 2.07 and 23.75 hours (mean 13.67 hours). Forty-three decedents were excluded from this study because of an excessive delay (>24 hours) between death and first MRI scanning opportunity (n = 18), negative reverse transcriptase PCR on nasopharyngeal swab specimen (n = 7), negative chest CT scan findings (n = 6), history of focal brain lesion (n = 10), or MRI incompatibility (n = 2).

The mean age of included decedents was 77 (range 49–94) years. All decedents had severe COVID-19 with 1 to 5 comorbid

Table 1 Decedents' characteristics

Age (range), y	77 (49–94)
Sex, F/M, n	5/14
Comorbid conditions, n (%)	
Hypertension	16/19 (84)
Cardiac disease	7/19 (37)
Diabetes mellitus	6/19 (32)
Chronic obstructive pulmonary disease	6/19 (32)
Malignancy	5/19 (26)
Body mass index, mean (range), kg/m^2	29 (18–42); 95% >25
Smoking	
Current smoker	0/19
Ex-smoker	5/19 (26)
Cognitive impairment	4/19 (21)
Symptoms on admission, n (%)	
Fever (>38.5°C)	5/19 (26)
Cough	10/19 (53)
Dyspnea	18/19 (95)
Gastrointestinal symptoms	4/19 (21)
CNS symptoms on admission, n (%)	
Headache	2/19 (10)
Agitation, confusion, disorientation	5/19 (26)
Seizure	1/19 (5; 2 d before admission)
Complications during hospital/intensive care unit stay, n (%)	
Respiratory failure	15/19 (79)
Acute kidney injury	14/19 (74)
Acute cardiac injury	18/19 (95)
Septic shock/multiple organ failure	4/19 (21)

conditions (i.e., hypertension, cardiac disorder, diabetes mellitus, chronic obstructive pulmonary disorder, chronic kidney disease, or body mass index >25 kg/m^2). Anosmia was not reported in any decedent, but it was not systematically assessed. Decedents developed typical COVID-19 complications such as coagulopathy (6 of 19), acute kidney injury (14 of 19), or acute cardiac injury (18 of 19). D-dimer level was abnormal in all tested decedents (11 of 19). The assessment of arterial hypertension before death was limited for most patients admitted to COVID-19 wards due to their respiratory distress and end-of-life status. Among the patients who died in the intensive care unit (ICU; decedent [D] 2, D8, D9, D15, D19), none had mean arterial pressure >100 mm Hg, and most of them received vasopressors before death to achieve at least 65–mm Hg mean arterial pressure. Mechanical ventilation was used in the 5 decedents hospitalized in the ICU, and 2 of them (D2 and D9) were placed on veno-venous extracorporeal membrane oxygenation. None of the 14 decedents hospitalized in COVID-19 wards benefited from mechanical ventilation. Fifteen decedents died of respiratory failure, while 4 died of septic shock and multiorgan failure. All decedents were on anticoagulation (therapeutic 6 of 19, prophylactic 13 of 19).

Brain MRI findings reflecting postmortem changes

Signal abnormalities consistent with early postmortem changes are detailed in table e-2 available from Dryad, doi.org/10.5061/dryad.4qrfj6q7p.

The increase in T1WI signal intensity, when present, did not involve homogeneously the basal ganglia and the thalami but was limited to the pallidi and posterolateral thalami (figure 1).

Figure 1 Algor mortis–related T1-weighted imaging increased signal intensity of deep nuclei

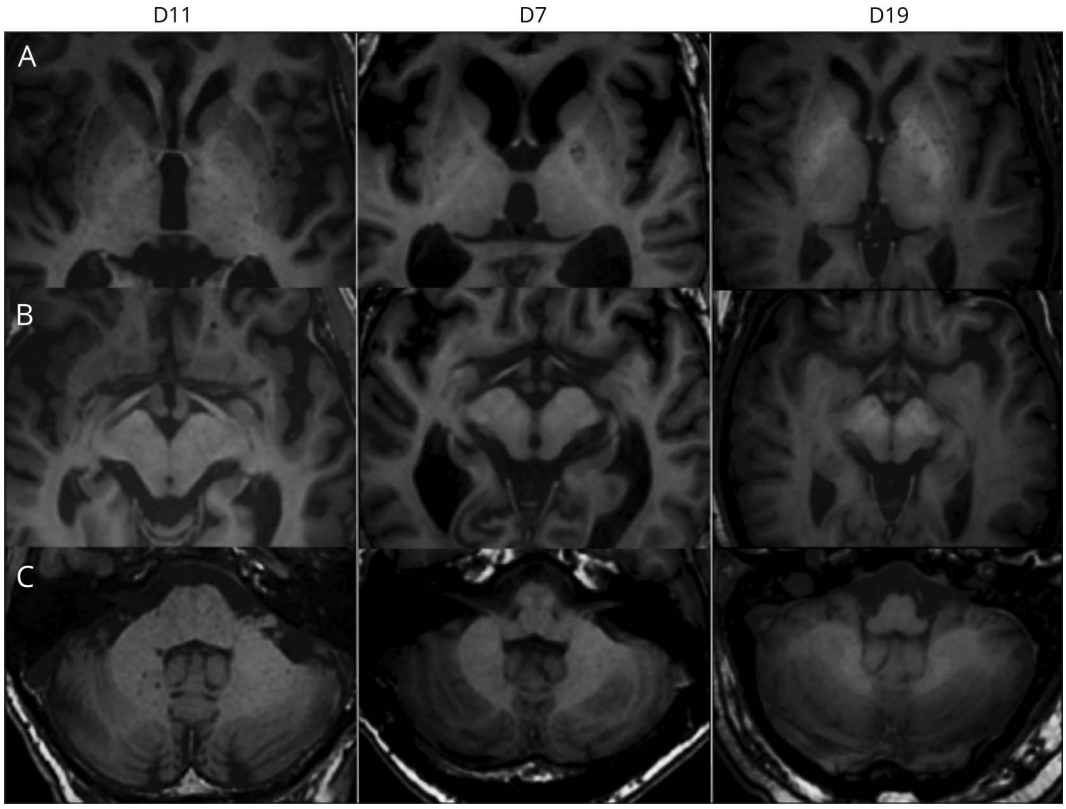

Zoomed axial slices centered on the (A) basal ganglia, (B) substantia nigra and red nuclei, and (C) dentate nuclei. In the first column (decedent [D] 11, scan delay 3.38 hours), no clear high T1 signal (grade 0) is visible in the deep nuclei. In the second column (D7, scan delay 5.05 hours), there is mildly (grade 1) increased T1 signal intensity in the substantia nigra and red nuclei. In the third column (D19, scan delay 18.40 hours), more marked (grade 2) T1 high signal is seen in the bilateral pallidi, posterolateral thalami, and substantia nigra, as well as in the red and dentate nuclei. Of note, there is focal signal decrease in the internal aspect of the pallidi in D7, consistent with mild, nonpathologic mineralization. All images are displayed in radiologic convention.

Moreover, a similar increase in T1WI signal intensity was also present in the substantia nigra, red nuclei, and dentate nuclei in many decedents (figure 1). These gray matter structures were thus included in the analysis of postmortem T1WI signal intensity changes in addition to the pallidal nuclei and posterolateral thalami. The only decedent (D11) who did not show clearly increased T1WI signal intensity in any of the above-mentioned deep nuclei was scanned after a delay of 3.38 hours, while decedents who had increased signal intensity in all these structures (D2, D8, D9, D10, D12, D16–D19) had a scan delay ranging from 14.90 hours (D12) to 23.75 hours (D16).

Suppression of fat on T2 WI was observed in all decedents. It was classified as complete (2) in 13 of 19 (mean scan delay 17.74 hours, range 4.35–23.75 hours) and incomplete (1) in 6 of 19 (4.85 hours, 2.07–12.28 hours) decedents (figure 2). There was in all cases some degree of marked subcutaneous fat suppression but not systematically in the deep orbital fat (figure 2).

On DWI, a cortical and periventricular high-signal-intensity rim was present in all decedents. It was classified as complete (2) in 15 of 19 decedents (mean scan delay 16.38 hours, range 2.80–23.75 hours) and incomplete (1) in 4 of 19 (3.51 hours, 2.07–5.05 hours; figure 3). A clear correspondence with ADC map or other sequence data was not found.

All decedents presented a diffuse reduction of ADC across the brain parenchyma. ADC values ranged from 152×10^{-6} mm^2/s (D10 and D17; scan delays of 18.75 and 21 hours, respectively) to 347×10^{-6} mm^2/s (D15; scan delay of 4.35 hours) in the left centrum semiovale, 216×10^{-6} mm^2/s (D10; 18.75 hours) to 503×10^{-6} mm^2/s (D11; 3.38 hours) in the left basal ganglia/thalamus, and 152×10^{-6} mm^2/s (D17; 21 hours) to 434×10^{-6} mm^2/s (D15; 4.35 hours) in the left cerebellum.

All decedents exhibited vascular signal loss on SWIs, some of them with increased visibility of vessels. The increased visibility of vessels was categorized as absent (0), discrete (1), moderate (2), or marked (3) on axial minimum intensity projections (10-mm thickness; figure 4). Increased visibility of vessels on SWI was categorized as absent (0) in 3 of 19 (scan delay range 17.10–22.37 hours), discrete (1) in 9 of 19 (scan delay range 3.52–23.75 hours), moderate (2) in 5 of 19 (scan delay range 2.07–18.40 hours), or marked (3) in 1 of 19 decedents (scan delay 20.13 hours).

Figure 2 Algor mortis–related fat suppression on T2-weighted imaging

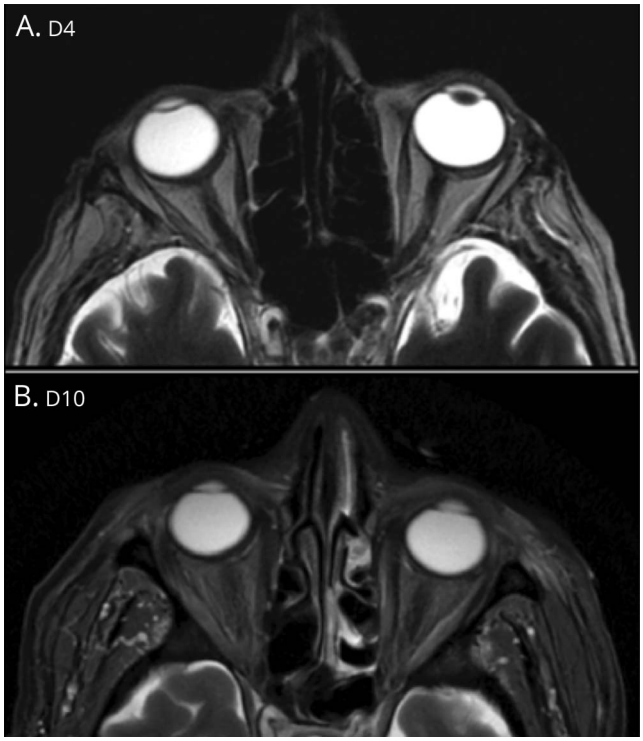

Axial images zoomed on the orbital region. (A) Decedent [D] 4, scan delay of 2.07 hours: clear fat signal suppression in the right subcutaneous fat and very mildly decreased signal intensity of orbital fat. (B) D10, scan delay of 18.75 hours: clear suppression of both subcutaneous and orbital fat. All images are displayed in radiologic convention.

Spearman rank correlation computations revealed significant negative correlations between scan delay and adjusted FLAIR TI ($\rho = -0.67$, $p = 0.0032$) and sum of the 3 ADC values ($\rho = -0.57$, $p = 0.0128$). Significant positive correlations were found with the sum of increased T1WI signal intensity scores ($\rho = 0.68$, $p = 0.0015$), T2WI fat suppression scores ($\rho = 0.76$, $p = 0.0001$), and DWI rim-like increased signal intensity score ($\rho = 0.61$, $p = 0.0053$). The correlation with SWI vessel visibility score ($\rho = -0.42$, $p = 0.08$) was not significant. All significant correlations survived Bonferroni correction (number of tests 6) except for the sum of ADC values.

Brain MRI findings reflecting antemortem changes

Recent and long-standing MRI signal changes are summarized in table e-3 available from Dryad, doi.org/10.5061/dryad.4qrfj6q7p. Figure 5 illustrates recent structural cerebral abnormalities in COVID-19 non-survivors. Parenchymal brain MRI abnormalities were found in 4 decedents.

D2 presented subcortical macrohemorrhages and microhemorrhages with posterior predominance, both supratentorially and infratentorially, which were best documented on SWI. The associated increased T1WI signal intensity in the larger lesions and overlying cortical edema suggested subacute hemorrhages (figures 5 and 6). A previous brain MRI, obtained in November 2016, did not show any hemorrhage. This decedent died in the ICU.

D4 exhibited 2 small arciform subcortical hemorrhages, 1 right temporal and 1 right occipital on SWI, corresponding to a discrete linear signal loss on T1WI and T2WI (figures 5 and 6). There was no surrounding vasogenic edema, microbleeds, or superficial hemosiderosis. White matter changes evocative of microvascular disease were limited, consisting of smooth periventricular hyperintensities, including caps around the ventricular horns and periventricular halos (Fazekas grade 1, figure 6). No antemortem MRI was available for this patient. D4 died 24 hours after admission and had systolic/diastolic blood pressure of 115/86 mm Hg at admission.

D7 showed superior precentral and parietal cortico-subcortical swelling associated with marked supratentorial white matter changes. The decedent's blood pressure measured 1 to 3 times a day in a COVID-19 ward oscillated between 90/55 and 140/80 mm Hg during the 5 days before death.

D9 had extensive T2WI hazy hyperintensity in bilateral centrum semiovale and was hospitalized in the ICU.

Four decedents had asymmetric olfactory bulbs with ipsilateral (D8) or without (D5, D11, D12) olfactory cleft obliteration. No other abnormality was found along the olfactory tract.

No signal abnormality was found in the brainstem except in D10, who had a midline pontine signal abnormality evocative of capillary telangiectasia (figure e-1 available from Dryad, doi.org/10.5061/dryad.4qrfj6q7p).

Discussion

In this case series of COVID-19 non-survivors, we performed a systematic and comprehensive assessment of the abnormalities encountered on their early postmortem brain MRI. Changes related to postmortem signal changes were analyzed first.[21–24] Then, antemortem changes were distinguished between presumed recent or chronic brain pathology with the use of common radiologic markers and scales.[26–29]

The present population of COVID-19 non-survivors was typical of those previously reported in the literature,[31–33] in particular regarding age, comorbid conditions, and complications leading to poor clinical outcome.

Five brain MRI findings were attributed to postmortem changes. The significant correlation between quantitative evaluation of these changes and the scan delay reinforced this hypothesis. These findings were (1) the necessary adaptation of the FLAIR TI to obtain adequate water suppression, (2) increased T1WI signal intensity of the deep nuclei, (3) T2WI fat suppression, (4) DWI rim-like increased signal intensity, and (5) decreased parenchymal ADC values. Overall, we attribute

Figure 3 Cortical and periventricular rim of increased DWI signal intensity

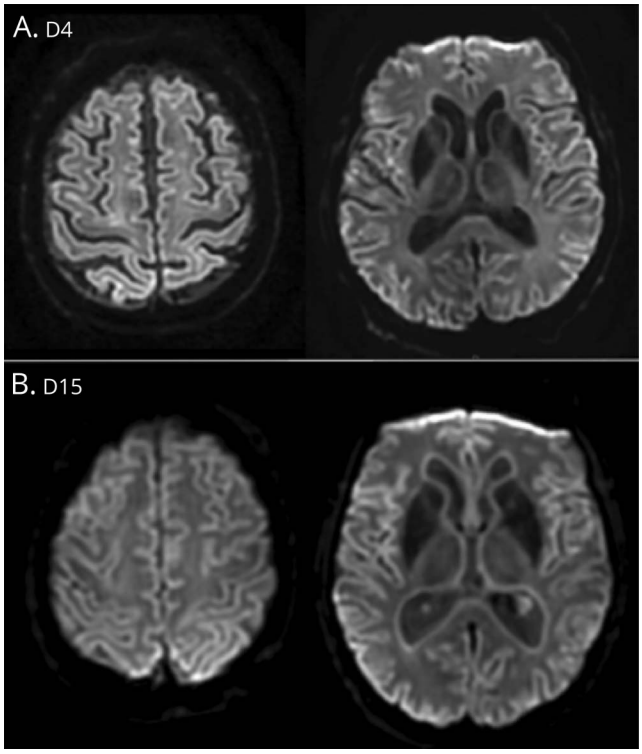

Postmortem rim-like high signal of the cortical ribbon and ventricular wall on diffusion-weighted imaging (DWI) was classified as (A) incomplete (decedent [D] 4, scan delay 2.07 hours) or (B) complete (D15, scan delay 16.77 hours). All images are displayed in radiologic convention.

those observations, at least partly, to the low temperature of decedent's body (algor mortis) compared to that in vivo, greatly influencing T1, and, to a lesser extent, T2 relaxation times.[34,35] These temperature changes were the common hypothesis formulated in existing postmortem literature,[21–24] which we reproduced in the above-mentioned brain findings.

One observation, the increased SWI vessel visibility, was not investigated in previous postmortem brain MRI reports and did not significantly correlate with scan delay. While it could still represent a postmortem change, the lack of correlation could be explained by a multiplicity of factors that may lead to such a phenomenon, for example, decrease in intravascular oxy/deoxyhemoglobin ratio, blood stagnation, decrease in brain temperature, and possible premortem intravascular clotting associated with the putative endothelial injury caused by SARS-CoV-2.[36] However, it was not present in the decedents with the most marked recent hemorrhagic (D2) or white matter (D9) changes and was only discretely present in the decedent with cortical edema (D7, grade 1). It therefore warrants further investigation.

The main limitation of the present postmortem MRI virtopsy lies in the severe SARS-CoV-2 pathology characterizing all decedents, which may limit the generalization of observed postmortem brain MRI findings to other clinical settings.

Parenchymal brain MRI abnormalities were observed in 4 of 19 decedents (21%), while asymmetric olfactory bulbs were found in 4 others (21%).

D2 had diffuse subcortical microbleeds and macrobleeds with posterior predominance. Considering his clinico-biological context, these abnormalities were evocative of multifocal hemorrhagic lesions triggered by DIC.[37,38] DIC is indeed frequently observed in patients with severe COVID-19.[37] Nevertheless, intracerebral hemorrhage is also a possible and rather frequent (5%–10% of patients) complication of extracorporeal membrane oxygenation, although diffuse microbleeds are seen only sporadically and do not display a posterior predominance.[39] A combination of different causes underlying intracranial hemorrhages in D2 therefore has to be considered, with blood-brain barrier breakdown possibly favored by SARS-CoV-2–related endothelial dysfunction as a hypothetical synergic pathophysiologic mechanism.

In D4, we observed 2 posterior macro-subcortical bleeds, which shared some similarities with those observed in D2. Their origin is arguably more difficult to interpret in the absence of a previous brain MRI. Still, we suspect that pathophysiologic mechanisms other than the classic SVD and CAA took place. SVD is associated with microbleeds and lacunes (posterior fossa, basal ganglia, supratentorial white matter), white matter hyperintensities, and cortical infarcts.[40,41] Hemorrhages due to CAA are associated with large lobar macrohemorrhage, lobar microbleeds,[25] cortical superficial siderosis,[42] white matter hyperintensities, and enlargement of perivascular spaces in the centrum semiovale.[43] D4 instead presented an isolated left thalamic lacune and very mild white matter hyperintensities (Fazekas grade 1) for his age (79 years), no enlargement of perivascular spaces, and no other hemorrhage. Although according to the modified Boston criteria[25] the diagnosis of CAA is deemed probable in the presence of 2 lobar bleeds, it is so in the absence of other causes of hemorrhage. Other possible causes could be head trauma (not reported and unlikely given the imaging appearance of the bleeds), hypertension (normal blood pressure at admission with death after 24 hours, intracranial hemorrhage more often located in deep brain structures and associated with radiologic signs of SVD[44]), anticoagulant therapy (prophylactic anticoagulation in this decedent), or blood clots (D-dimer level not available). Considering the COVID-19 status of the decedent, it might be hypothesized that these 2 subcortical hemorrhages were triggered by blood-brain barrier breakdown phenomena similar to those in D2.

D7 showed superior precentral and parietal cortico-subcortical swelling associated with marked supratentorial white matter changes. These findings are evocative of posterior reversible encephalopathy syndrome (PRES). PRES refers to reversible vasogenic brain edema predominating in posterior brain regions, which occurs in association with a variety of systemic disorders.[45,46] PRES is typically caused by endothelial injury related to abrupt blood pressure changes or direct effects of cytokines on the endothelium.[45,46] In D7, the blood pressure monitored during her stay in a COVID-19 ward did not support

Figure 4 Postmortem increased vessel visibility on SWI sequence

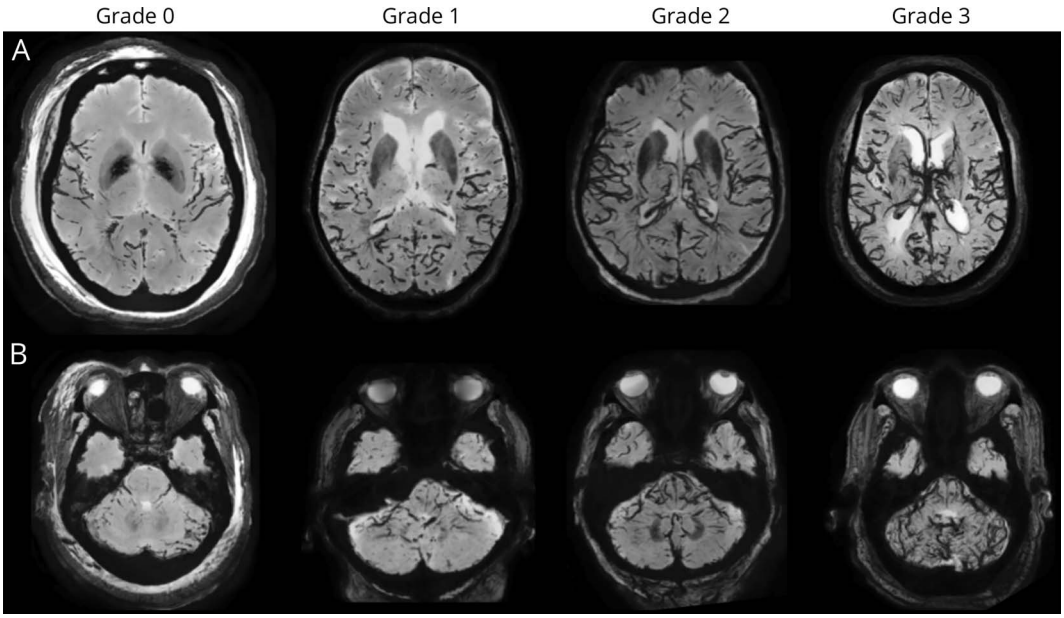

The grading system developed in this study for vessel visibility is illustrated for each grade by (A) supratentorial and (B) infratentorial images on axial minimum intensity projections (10 mm thick). First column: no dilatation, grade 0 (decedent [D] 9, scan delay 17.10 hours), apparent caliber of vessels on susceptibility-weighted imaging (SWI) is similar to that in vivo. Second column: discrete, grade 1 (D3, scan delay 17.82 hours), slightly increased conspicuity of superficial vessels. Third column: moderate, grade 2 (D4, scan delay 2.07 hours); and fourth column: marked, grade 3 (D1, scan delay 20.13 hours), visibility of superficial vessels is increased and deep perforating vessels become gradually apparent from grade 2 to 3. All images are displayed in radiologic convention.

the hypothesis that hypertension was at the origin of PRES in her case. PRES has been reported in patients with normal blood pressure or hypotension.[45,46] In those patients, endothelial dysfunction from, for example, the cytotoxic effects of infection (e.g., cytokine storm) is one of the considered pathophysiologic mechanisms.[45,46] PRES has been reported in a young adult with COVID-19 who developed acute confusional state and transient cortical blindness.[47] PRES should therefore be considered a potential complication of COVID-19.

D9 had extensive hazy T2WI hyperintensity of the centrum semiovale of uncertain significance. This could be the manifestation of early edematous changes due to blood-brain barrier breakdown associated with hypoxia or deep watershed infarction. Still, unspecific chronic changes related to the decedent's metabolic disorders (hyperthyroidism and hyperaldosteronism) cannot be excluded. Such hazy white matter T2WI hyperintensity has been reported in 37% of patients with COVID-19 with neurologic symptoms admitted to the ICU, for whom a definite diagnosis was difficult to determine.[48]

In those 4 decedents with parenchymal brain MRI abnormalities, blood-brain barrier breakdown might be the common denominator among DIC-related lesions, PRES, and centrum semiovale changes.[49] It might be caused by endothelial dysfunction related to severe COVID-19 (i.e., severe hypoxia, DIC, cytokine storm) with or without direct SARS-CoV-2 infection of endothelial cells. Given the widespread endothelial expression of ACE2,[36] such hypothetical endothelial infection might lead to secondary intracerebral endothelial inflammation and activation. Both cytokine storm and SARS-CoV-2 infection of endothelial cells occur in severe COVID-19, leading to a widespread endotheliitis.[36] Of note, we did not find in our series larger ischemic[13] or hemorrhagic[12] strokes, which have previously been reported in COVID-19. This absence of large ischemic stroke may result from the widespread use of prophylactic or therapeutic anticoagulation in all decedents. This study therefore enlarges the clinical spectrum of possible vascular changes that can be found in patients with severe COVID-19.

Asymmetric olfactory bulbs with or without olfactory cleft obliteration were observed in 4 of 19 decedents. This may represent an MRI correlate of anosmia frequently observed in patients with SARS-CoV-2 and may support the neural retrograde hypothesis for SARS-CoV-2 CNS dissemination. Still, anosmia was not reported in any of the decedents, but it was not systematically assessed, and this study did not find any MRI signal abnormality downstream from the olfactory tract. Normal olfactory bulb and tract with no sign of nasal congestion have been reported in 1 SARS-CoV-2–infected patient with acute anosmia.[8] Further studies are warranted to better understand the pathophysiologic mechanisms of anosmia in COVID-19.

This study failed to find specific brainstem abnormalities, bringing no support to a brain-related contribution to respiratory distress in COVID-19.[6] Still, this does not exclude the possibility of SARS-CoV-2-related dysregulation of brainstem respiratory nuclei not observable on brain MRI.

Figure 5 Postmortem brain MRI findings in 5 decedents (D2, D4, D7, D8, D9)

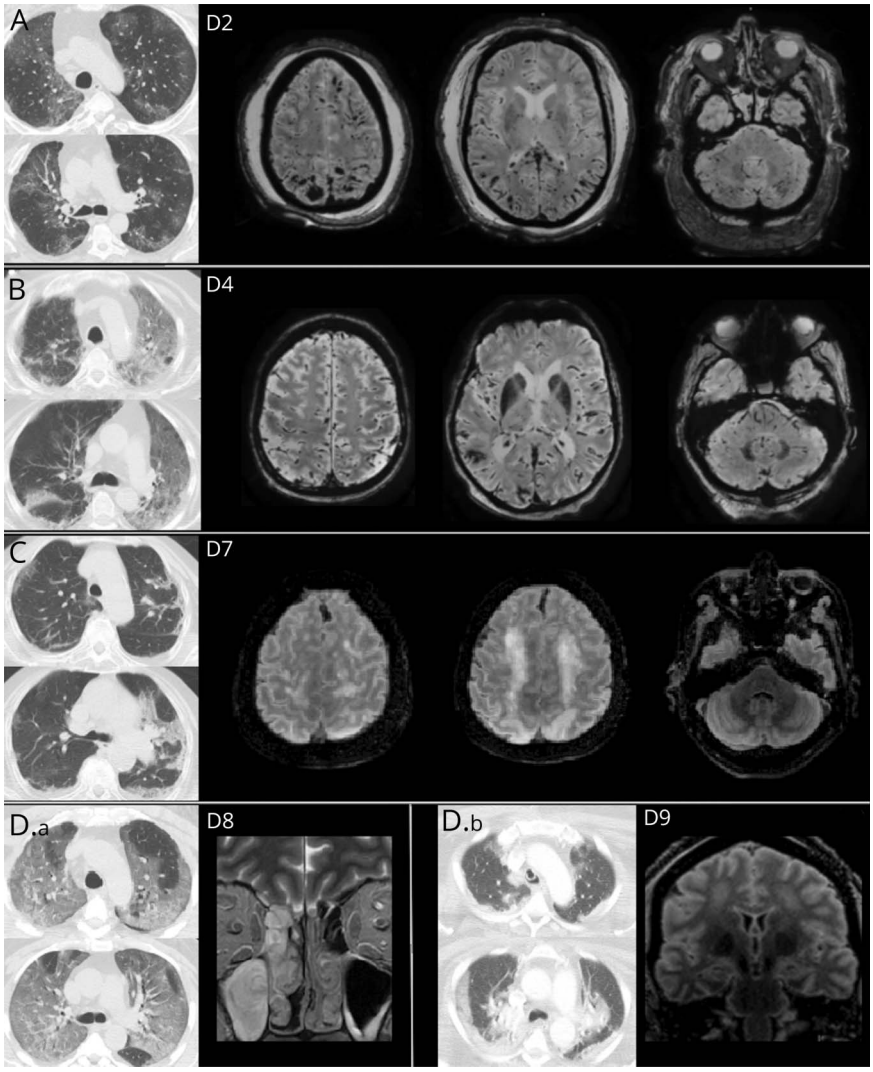

For each decedent, 2 axial slices of their chest CT scan (first 2 images on the left) are provided to illustrate the typical severe acute respiratory syndrome coronavirus 2–related ground-glass multifocal lung opacities (delay between chest CT scan and death: decedent [D] 2, 10 days; D4, 1 day; D7, 7 days; D8, 21 days; D9, 2 days). (A) D2 had diffuse microbleeds and macrobleeds with parieto-occipito-temporal predominance, also involving the splenium of corpus callosum, left superior frontal sulcus, and bilateral cerebellum, as demonstrated on the susceptibility-weighted imaging (SWI) sequence. (B) D4 presented with 2 isolated arciform subcortical macrobleeds in the right occipital and temporal lobes, also visible on the SWI sequence. (C) D7 displayed cortical and subcortical high fluid-attenuated inversion recovery (FLAIR) signal intensity and swelling in the bilateral superior precentral gyri and superior parietal lobules, while the posterior fossa was spared. (D.a) D8 had a relatively tumefied left olfactory bulb associated with ipsilateral obliteration of the olfactory cleft. (D.b) D9 showed bilateral, extensive, and hazy FLAIR high signal intensity of the bilateral centrum semiovale. All images are displayed in radiologic convention.

Our study has some limitations. First, due to our strict inclusion criteria, 70% of patients with COVID-19 who died during the inclusion period at our institution were not included in the present study. Due to this high-level of exclusion, the study may not provide a complete picture of COVID-19–related brain MRI abnormalities. In particular, we included only decedents with positive detection of SARS-CoV-2 on nasopharyngeal swab specimen and a chest CT scan typical of COVID-19 to reinforce the possible associations between postmortem brain MRI findings and COVID-19 or its complications. Due to this stringent inclusion criterion, the study does not investigate the possible occurrence of brain lesions in SARS-CoV-2–infected decedents without pulmonary involvement (see, e.g., the work by Inciardi et al.[50]). We limited the delay between death and postmortem MRI data acquisition to <24 hours to reduce the effects of postmortem brain changes that could complicate the interpretation of brain MRI data.[21,22] The strong correlations found between the delay and the evolution of brain MRI signal support this approach. We decided to exclude decedents with known focal brain lesions because they could complicate the interpretation of postmortem brain MRI data. Previously lesioned brain tissue may indeed represent an easier way for the virus to enter the brain due to, for example, blood-brain barrier breakdown. This might complicate the interpretation of the recent vs long-lasting origin of antemortem brain MRI abnormalities.

Second, several limitations are intrinsic to the virtopsy approach used in this study. Interpretations of brain MRI findings are indeed complicated by (1) postmortem brain changes (see above), (2) the global reduction of ADC that limits the use of this information for DWI data interpretation, and (3) the lack of circulation, preventing the use of both exogenous (gadolinium) and endogenous (e.g., blood oxygen level–dependent signal, arterial spin labeling, time-of-flight angiography) tracers.[21,22] These intrinsic limitations forced us to adopt a systematic and descriptive approach to report the brain MRI findings and to provide prudent interpretation of those attributed to COVID-19, after reaching a multidisciplinary consensus.

Figure 6 Additional illustrations for (A) D2 and (B) D4

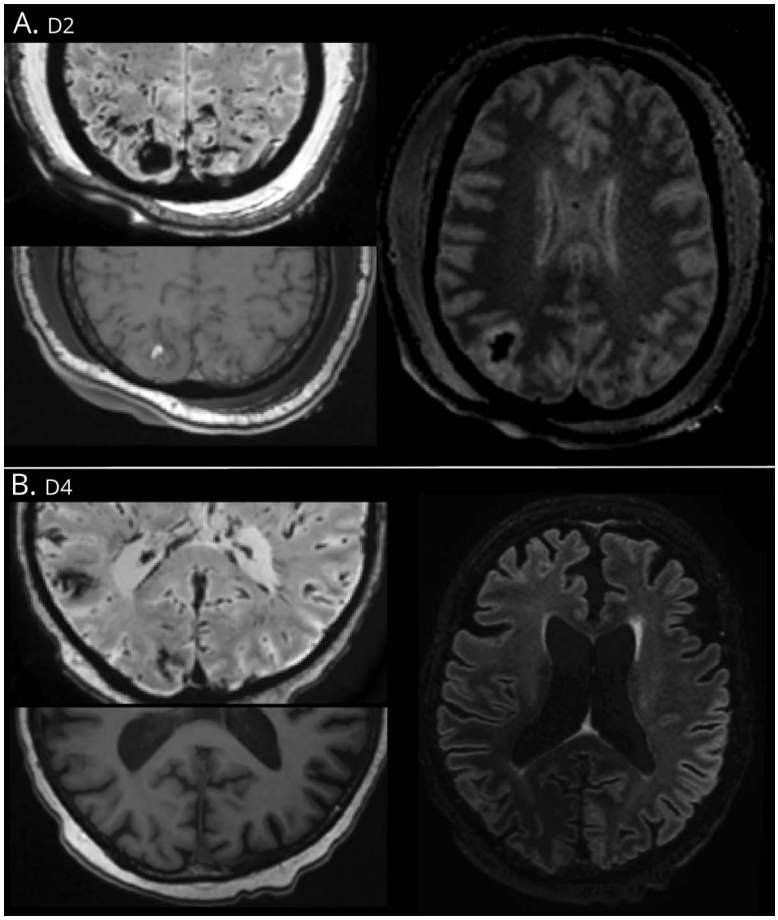

Subcortical hemorrhagic lesions are depicted on the left in susceptibility-weighted imaging (SWI) and T1-weighted imaging (T1WI) axial image pairs. The right parietal macrohemorrhage of D2 presented a clear T1WI hyperintensity, while it is not the case for D4 and the smaller hemorrhagic lesions of D2. Reformatted axial fluid-attenuated inversion recovery (FLAIR) images on the right show mild cortical edema overlying another right parietal macrohemorrhage in D2. D2 did not present white matter changes, and D4 had only weak FLAIR signal changes in the periventricular white matter (Fazekas grade 1) with limited atrophy and no microbleed. All images are displayed in radiologic convention.

Third, the design of this study was prospective in the sense that consecutive decedents fulfilling inclusion criteria during the inclusion period were all included in a prospective manner. The inclusion process therefore started at the time of death. This implied that, during the hospitalization, patients' clinical status was not systematically investigated in light of the objectives of the study. We relied on the medical records for information about decedents' neurologic status. With the high pressure of the COVID-19 outbreak on medical facilities and staff, stress was put on patients' respiratory and systemic status. Thus, the neurologic status was not reported with full detail in the critically ill or end-of-life patients such as the included decedents.

Finally, because this study focused on COVID-19 non-survivors, it did not evaluate patients with COVID-19 and acute neurologic symptoms (e.g., stroke, seizures, etc.) who survived. This study therefore provides an incomplete picture of COVID-19–related brain disorders such as those previously reported and not found in this case series.[11,12,14] Still, this study provides insights into the possible types of brain lesions that can be observed in COVID-19.

Acknowledgment

The authors express their most sincere gratitude to all the personnel of the morgue and of the PET-MR Unit of the CUB Hôpital Erasme. Their fantastic work and efforts made this study possible.

Study funding

This work was supported by a special call "COVID-19" funded by the Université libre de Bruxelles, the Fonds Erasme (Brussels, Belgium), and the Fondation ULB (Brussels, Belgium). The PET-MR project at the CUB Hôpital Erasme and Université libre de Bruxelles is financially supported by the Association Vinçotte Nuclear (Brussels, Belgium). T.C. is clinical master specialist applicant to a PhD at the Fonds de la Recherche Scientifique (FRS-FNRS; Brussels, Belgium). G.N. and X.D.T. are postdoctorate clinical master specialists at the FRS-FNRS (Brussels, Belgium).

Disclosure

The authors report no disclosures relevant to the manuscript. Go to Neurology.org/N for full disclosures.

Publication history

A preprint of this article (without the supplementary material) has been uploaded to the MedRxiv server (https://medrxiv.org/cgi/content/short/2020.05.04.20090316v1). Received by *Neurology* May 8, 2020. Accepted in final form June 9, 2020.

Appendix Authors

Name	Location	Contribution
Tim Coolen, MD	Department of Radiology, CUB Hôpital Erasme, Université libre de Bruxelles (ULB), Brussels, Belgium; Laboratoire de Cartographie fonctionnelle du Cerveau, UNI–ULB Neuroscience Institute, ULB, Brussels, Belgium	Study concept and design; data analysis; interpretation of data; full access to all of the data in the study; responsible for the integrity of the data and the accuracy of the data analysis; statistical analyses; drafting the manuscript; critical revision of the manuscript for important intellectual content; shares first authorship with equal contributions
Valentina Lolli, MD	Department of Radiology, CUB Hôpital Erasme, Université libre de Bruxelles (ULB), Brussels, Belgium; Laboratoire de Cartographie fonctionnelle du Cerveau, UNI–ULB Neuroscience Institute, ULB, Brussels, Belgium	Study concept and design; data analysis; interpretation of data; full access to all of the data in the study; responsible for the integrity of the data and the accuracy of the data analysis; drafting the manuscript; critical revision of the manuscript for important intellectual content; shares first authorship with equal contributions
Niloufar Sadeghi, MD, PhD	Department of Radiology, CUB Hôpital Erasme, Université libre de Bruxelles, Brussels, Belgium	Study concept and design; data analysis; interpretation of data; full access to all of the data in the study; responsible for the integrity of the data and the accuracy of the data analysis; drafting the manuscript; critical revision of the manuscript for important intellectual content.
Antonin Rovaï, PhD	Laboratoire de Cartographie fonctionnelle du Cerveau, UNI–ULB Neuroscience Institute, Université libre de Bruxelles (ULB), Brussels, Belgium; Department of Nuclear Medicine, CUB Hôpital Erasme, ULB, Brussels, Belgium	Interpretation of data; critical revision of the manuscript for important intellectual content
Nicola Trotta, PhD	Laboratoire de Cartographie fonctionnelle du Cerveau, UNI–ULB Neuroscience Institute, Université libre de Bruxelles (ULB), Brussels, Belgium; Department of Nuclear Medicine, CUB Hôpital Erasme, ULB, Brussels, Belgium	Interpretation of data; critical revision of the manuscript for important intellectual content
Fabio Silvio Taccone, MD, PhD	Intensive Care Unit, CUB Hôpital Erasme, Université libre de Bruxelles, Brussels, Belgium	Interpretation of data; critical revision of the manuscript for important intellectual content
Jacques Creteur, MD, PhD	Intensive Care Unit, CUB Hôpital Erasme, Université libre de Bruxelles, Brussels, Belgium	Interpretation of data; critical revision of the manuscript for important intellectual content
Sophie Henrard, MD	Department of Internal Medicine, CUB Hôpital Erasme, Université libre de Bruxelles, Brussels, Belgium	Interpretation of data; critical revision of the manuscript for important intellectual content
Jean-Christophe Goffard, MD, PhD	Department of Internal Medicine, CUB Hôpital Erasme, Université libre de Bruxelles, Brussels, Belgium	Interpretation of data; critical revision of the manuscript for important intellectual content
Olivier De Witte, MD, PhD	Department of Neurosurgery, CUB Hôpital Erasme, Université libre de Bruxelles, Brussels, Belgium	Study concept and design; interpretation of data; critical revision of the manuscript for important intellectual content
Gilles Naeije, MD, PhD	Department of Nuclear Medicine, CUB Hôpital Erasme, Université libre de Bruxelles (ULB), Brussels, Belgium; Department of Neurology, CUB Hôpital Erasme, ULB, Brussels, Belgium	Interpretation of data; drafting the manuscript; critical revision of the manuscript for important intellectual content
Serge Goldman, MD, PhD	Laboratoire de Cartographie fonctionnelle du Cerveau, UNI–ULB Neuroscience Institute, Université libre de Bruxelles (ULB), Brussels, Belgium; Department of Nuclear Medicine, CUB Hôpital Erasme, ULB, Brussels, Belgium	Study concept and design; data acquisition and analysis; interpretation of data; full access to all of the data in the study; responsible for the integrity of the data and the accuracy of the data analysis; drafting the manuscript; critical revision of the manuscript for important intellectual content; obtained funding
Xavier De Tiège, MD, PhD	Laboratoire de Cartographie fonctionnelle du Cerveau, UNI–ULB Neuroscience Institute, Université libre de Bruxelles (ULB), Brussels, Belgium; Department of Nuclear Medicine, CUB Hôpital Erasme, ULB, Brussels, Belgium	Study concept and design; data acquisition and analysis; interpretation of data; full access to all of the data in the study; responsible for the integrity of the data and the accuracy of the data analysis; drafting the manuscript; critical revision of the manuscript for important intellectual content; obtained funding

References

1. Zhu N, Zhang D, Wang W, et al. A novel coronavirus from patients with pneumonia in China, 2019. N Engl J Med 2020;382:727–733.
2. Zhou P, Yang X-L, Wang X-G, et al. A pneumonia outbreak associated with a new coronavirus of probable bat origin. Nature 2020;579:270–273.
3. Walls AC, Park Y-J, Tortorici MA, Wall A, McGuire AT, Veesler D. Structure, function, and antigenicity of the SARS-CoV-2 spike glycoprotein. Cell Epub 2020 Mar 6.

4. Xia H, Lazartigues E. Angiotensin-converting enzyme 2 in the brain: properties and future directions. J Neurochem 2008;107:1482–1494.
5. De Felice FG, Tovar-Moll F, Moll J, Munoz DP, Ferreira ST. Severe acute respiratory syndrome coronavirus 2 (SARS-CoV-2) and the central nervous system. Trends Neurosci Epub 2020 Apr 21.
6. Li Y-C, Bai W-Z, Hashikawa T. The neuroinvasive potential of SARS-CoV2 may play a role in the respiratory failure of COVID-19 patients. J Med Virol Epub 2020 Feb 27.
7. Spinato G, Fabbris C, Polesel J, et al. Alterations in smell or taste in mildly symptomatic outpatients with SARS-CoV-2 infection. JAMA Epub 2020 Apr 22.
8. Galougahi MK, Ghorbani J, Bakhshayeshkaram M, Naeini AS, Haseli S. Olfactory bulb magnetic resonance imaging in SARS-CoV-2-induced anosmia: the first report. Acad Radiol 2020;27:892–893
9. Huang YH, Hanna Huang Y, Jiang D, Huang JT. SARS-CoV-2 detected in cerebrospinal fluid by PCR in a case of COVID-19 encephalitis. Brain Behav Immun Epub 2020 May 6.
10. Ye M, Ren Y, Lv T. Encephalitis as a clinical manifestation of COVID-19. Brain Behav Immun Epub 2020 Apr 10.
11. Moriguchi T, Harii N, Goto J, et al. A first case of meningitis/encephalitis associated with SARS-coronavirus-2. Int J Infect Dis Epub 2020 Apr 3.
12. Sharifi-Razavi A, Karimi N, Rouhani N. COVID 19 and Intra cerebral hemorrhage: causative or coincidental. New Microbes New Infect 2020;35:100669.
13. Oxley TJ, Mocco J, Majidi S, et al. Large-vessel stroke as a presenting feature of covid-19 in the young. N Engl J Med 2020;382:e60.
14. Poyiadji N, Shahin G, Noujaim D, Stone M, Patel S, Griffith B. COVID-19-associated acute hemorrhagic necrotizing encephalopathy: CT and MRI features. Radiology Epub 2020 Mar 31.
15. Mao L, Jin H, Wang M, et al. Neurologic manifestations of hospitalized patients with coronavirus disease 2019 in Wuhan, China. JAMA Neurol Epub 2020 Apr 10.
16. Kellum JA, Lameire N; KDIGO AKI Guideline Work Group. Diagnosis, evaluation, and management of acute kidney injury: a KDIGO summary (part 1). Crit Care 2013; 17:204.
17. Henrion J. Hypoxic hepatitis. Liver Int 2012;32:1039–1052.
18. Taylor F, Toh C-H, Hoots K, Wada H, Levi M. Towards definition, clinical and laboratory criteria, and a scoring system for disseminated intravascular coagulation. Thromb Haemost 2001;86:1327–1330.
19. Shi S, Qin M, Shen B, et al. Association of cardiac injury with mortality in hospitalized patients with COVID-19 in Wuhan, China. JAMA Cardiol Epub 2020 Mar 25.
20. Tofts PS, Jackson JS, Tozer DJ, et al. Imaging cadavers: cold FLAIR and noninvasive brain thermometry using CSF diffusion. Magn Reson Med 2008;59:190–195.
21. Offiah CE, Dean J. Post-mortem CT and MRI: appropriate post-mortem imaging appearances and changes related to cardiopulmonary resuscitation. Br J Radiol 2016; 89:20150851.
22. Grabherr S, Egger C, Vilarino R, Campana L, Jotterand M, Dedouit F. Modern post-mortem imaging: an update on recent developments. Forensic Sci Res 2017;2:52–64.
23. Wagensveld IM, Blokker BM, Wielopolski PA, et al. Total-body CT and MR features of postmortem change in in-hospital deaths. PLoS One 2017;12:e0185115.
24. Kobayashi T, Shiotani S, Kaga K, et al. Characteristic signal intensity changes on postmortem magnetic resonance imaging of the brain. Jpn J Radiol 2010;28: 8–14.
25. Greenberg SM, Charidimou A. Diagnosis of cerebral amyloid angiopathy: evolution of the Boston criteria. Stroke 2018;49:491–497.
26. Fazekas F, Chawluk JB, Alavi A, Hurtig HI, Zimmerman RA. MR signal abnormalities at 1.5 T in Alzheimer's dementia and normal aging. Am J Roentgenology 1987;149: 351–356.
27. Maclullich AMJ, Wardlaw JM, Ferguson KJ, Starr JM, Seckl JR, Deary IJ. Enlarged perivascular spaces are associated with cognitive function in healthy elderly men. J Neurol Neurosurg Psychiatry 2004;75:1519–1523.
28. Doubal FN, MacLullich AMJ, Ferguson KJ, Dennis MS, Wardlaw JM. Enlarged perivascular spaces on MRI are a feature of cerebral small vessel disease. Stroke 2010; 41:450–454.
29. Harper L, Barkhof F, Fox NC, Schott JM. Using visual rating to diagnose dementia: a critical evaluation of MRI atrophy scales. J Neurol Neurosurg Psychiatry 2015;86: 1225–1233.
30. Ng SES, Low AMS, Tang KK, Chan YH, Kwok RK. Value of quantitative MRI biomarkers (Evans' index, aqueductal flow rate, and apparent diffusion coefficient) in idiopathic normal pressure hydrocephalus. J Magn Reson Imaging 2009;30:708–715.
31. Du R-H, Liang L-R, Yang C-Q, et al. Predictors of mortality for patients with COVID-19 pneumonia caused by SARS-CoV-2: a prospective cohort study. Eur Respir J Epub 2020 Jan 1.
32. Guan W-J, Liang W-H, He J-X, Zhong N-S. Cardiovascular comorbidity and its impact on patients with COVID-19. Eur Respir J 2020;55:2001227.
33. Zhou F, Yu T, Du R, et al. Clinical course and risk factors for mortality of adult inpatients with COVID-19 in Wuhan, China: a retrospective cohort study. Lancet 2020;395:1054–1062.
34. Nelson TR, Tung SM. Temperature dependence of proton relaxation times in vitro. Magn Reson Imaging 1987;5:189–199.
35. Zech W-D, Schwendener N, Persson A, Warntjes MJ, Jackowski C. Temperature dependence of postmortem MR quantification for soft tissue discrimination. Eur Radiol 2015;25:2381–2389.
36. Varga Z, Flammer AJ, Steiger P, et al. Endothelial cell infection and endotheliitis in COVID-19. Lancet Epub 2020 Apr 20.
37. Lillicrap D. Disseminated intravascular coagulation in patients with 2019-nCoV pneumonia. J Thromb Haemost 2020;18:786–787.
38. Lucas A. Disseminated intravascular coagulation: the hemorrhagic hurricane and the cytokine storm. J Clin Exp Cardiol 20134:1000e127.
39. Luyt C-E, Bréchot N, Demondion P, et al. Brain injury during venovenous extracorporeal membrane oxygenation. Intensive Care Med 2016;42:897–907.
40. Wardlaw JM, Smith C, Dichgans M. Small vessel disease: mechanisms and clinical implications. Lancet Neurol 2019;18:684–696.
41. Staals J, Makin SDJ, Doubal FN, Dennis MS, Wardlaw JM. Stroke subtype, vascular risk factors, and total MRI brain small-vessel disease burden. Neurology 2014;83:1228–1234.
42. Charidimou A, Jäger RH, Fox Z, et al. Prevalence and mechanisms of cortical superficial siderosis in cerebral amyloid angiopathy. Neurology 2013;81:626–632.
43. Charidimou A, Boulouis G, Pasi M, et al. MRI-visible perivascular spaces in cerebral amyloid angiopathy and hypertensive arteriopathy. Neurology 2017;88:1157–1164.
44. Caceres JA, Goldstein JN. Intracranial hemorrhage. Emerg Med Clin North Am 2012; 30:771–794.
45. Fugate JE, Rabinstein AA. Posterior reversible encephalopathy syndrome: clinical and radiological manifestations, pathophysiology, and outstanding questions. Lancet Neurol 2015;14:914–925.
46. Hinduja A. Posterior reversible encephalopathy syndrome: clinical features and outcome. Front Neurol 2020;11:71.
47. Kaya Y, Kara S, Akinci C, Kocaman AS. Transient cortical blindness in COVID-19 pneumonia; a PRES-like syndrome: case report. J Neurol Sci 2020;413:116858.
48. Kandemirli SG, Dogan L, Sarikaya ZT, et al. Brain MRI findings in patients in the intensive care unit with COVID-19 infection. Radiology Epub 2020 May 8.
49. Stokum JA, Gerzanich V, Marc Simard J. Molecular pathophysiology of cerebral edema. J Cereb Blood Flow Metab 2016;36:513–538.
50. Inciardi RM, Lupi L, Zaccone G, et al. Cardiac involvement in a patient with coronavirus disease 2019 (COVID-19). JAMA Cardiol Epub 2020 Mar 27.

Early postmortem brain MRI findings in COVID-19 non-survivors

Tim Coolen, Valentina Lolli, Niloufar Sadeghi, et al.

Neurology 2020;95;e2016-e2027 Published Online before print June 16, 2020
DOI 10.1212/WNL.0000000000010116